



Full length article

On the interaction of solute atoms with vacancies in diluted Al-alloys: A paradigmatic experimental and *ab-initio* study on indium and tin



Mohamed Elsayed^{a,b,*}, Torsten E.M. Staab^c, Jakub Čížek^d, Reinhard Krause-Rehberg^a

^a Department of Physics, Martin Luther University Halle, Halle 06099, Germany

^b Department of Physics, Faculty of Science, Minia University, Minia 61519, Egypt

^c Department of Chemistry and Pharmacy, Julius-Maximilians University Wuerzburg, LCTM, Roentgenring 11, Wuerzburg 97070, Germany

^d Faculty of Mathematics and Physics, Charles University, V Holešovičkách 2, CZ-180 00 Praha 8, Czech Republic

ARTICLE INFO

Article history:

Received 21 April 2021

Revised 27 July 2021

Accepted 31 July 2021

Available online 10 August 2021

Keywords:

positron annihilation spectroscopy

ab-initio calculations

Al alloys

In and Sn trace elements

isochronal annealing

vacancy-solute-atoms binding energy

ABSTRACT

To study the vacancy-solute-atom interaction, diluted Al-In and Al-Sn alloys with 0.005 and 0.025 at.% indium/tin cast from very high purity elements were investigated by positron annihilation spectroscopy (PAS). Therefore, the alloys have been solution heat treated at temperatures ranging from 320 to 620 °C and then rapidly quenched into ice water freezing-in most thermal vacancies. Positron annihilation lifetime (PALS) and coincidence Doppler broadening spectroscopies (CDBS) were combined to unambiguously identify vacancy-solute-atom complexes. For enabling a direct comparison to experiment, we did employ *ab-initio* DFT calculations of vacancy-solute-atom complexes providing relaxed atomic coordinates, which are used to calculate PAS annihilation parameters. In the as-quenched state vacancy-solute-atom pairs as well as vacancy clusters were observed in both alloys for all concentrations. During isochronal annealing vacancy clusters, formed during quenching, dissolved at about 130 °C, leaving vacancy-solute-atoms complexes as the only remaining defects. Thus, we could unambiguously identify those by a combination of PALS and CDBS with *ab-initio* calculations. Employing isothermal annealing the binding energy E_B of vacancies to In and Sn solute atoms was determined experimentally by PALS as well as by *ab-initio* calculations. We find from our experiments $E_B = (0.20 \pm 0.03)$ and (0.32 ± 0.10) eV for In and Sn, respectively, which is in very good agreement with our *ab-initio* calculations giving 0.23 and 0.26 eV, respectively. Our results clearly identified vacancy-In/Sn complexes as responsible for the retardation of vacancy migration after quenching. The vacancies bound to In and Sn solute-atoms are released around 150 °C shifting, when added to AlCu alloys as trace elements, the transport of copper atoms to higher temperatures necessary for the formation of finely distributed "precipitates", which efficiently strengthen this kind of alloys.

© 2021 The Authors. Published by Elsevier Ltd on behalf of Acta Materialia Inc.

This is an open access article under the CC BY license (<http://creativecommons.org/licenses/by/4.0/>)

1. Introduction

Pure aluminum has a relatively low tensile strength but alloying it with other elements like copper increases its strength by precipitation hardening, which is the most effective mechanism of strengthening aluminum alloys [1]. The highest strength of aluminum alloys is attributed to the formation of an evenly distributed high number density of small, nanometer sized particles formed by solid-state precipitation. Typically, this requires elevated temperature (120–200 °C) aging [2].

The addition of trace elements in the order of 100 ppm (microalloying) to aluminum and its alloy series AA-2xxx (Al-Cu) or AA-6xxx (Al-Mg-Si) is a standard process to optimize the material's mechanical properties by favorably influencing the decomposition kinetics and, thus, the precipitation process, which results in increasing the peak hardness [3–5].

Without understanding the role of vacancies, it has been discovered long time ago when using elements from the fifth group in the periodic table in diluted Al-In, Al-Sn, and Al-Cd pure binary alloys as well as additions to Al-Cu alloys that these elements retard the decomposition process at room temperature (RT) and suppress the formation of e.g. Guinier-Preston (GP-I) zones in Al-Cu alloys [6,7].

Nowadays, it is widely accepted that quenched-in vacancies strongly bound to solute atoms at RT will not participate in the

* Corresponding author at: Department of Physics, Martin Luther University Halle, Halle 06099, Germany.

E-mail address: mohamed.elsayed@physik.uni-halle.de (M. Elsayed).

decomposition of the solid solution until they are released at elevated temperatures. Vacancies do strongly bind to solute atoms like In, Sn or Cd forming vacancy-solute-atom complexes stable at RT. They typically remain thermally stable up to about 150 °C, and, thus, they hinder the migration of vacancies and shift the precipitation formation to an often more favorable temperature range. However, the exact geometry and composition of the complexes is unknown so far. Subsequently, at this elevated temperature the vacancy-solute-atom complexes are assumed to dissociate and release the formerly bound vacancies, which enhance the diffusion of other solute atoms and facilitate the formation of a high number density of small precipitates, e.g., Θ' in age-hardenable Al-Cu alloys [8–10].

Therefore, in recent years elements like indium and tin have often been added in trace element concentration to binary Al-Cu and ternary Al-Mg-Si alloys in order to improve their strength – see [10–15] and [16–18], respectively. However, the modified decomposition process in Al-Cu and Al-Mg-Si alloys containing low concentrations (up to a few 100 ppm) of trace elements is on the basis of atomic interactions so far only superficially understood.

Since most of the alloying elements in aluminum are substitutional and, thus, their diffusion occurs via the vacancy mechanism [19], i.e. by vacancy-solute-atom interactions, it is important to study the interaction of these trace element atoms with quenched-in vacancies by determining the vacancy-solute-atom binding energy, since the retardation of the decomposition depends on its magnitude, where various elements interact very differently with vacancies. However, there is only one experimental method able to directly detect vacancies or vacancy-solute-atom complexes in metals and alloys: positron annihilation spectroscopy (PAS) [20]. Positron annihilation spectroscopy is not only a well-suited tool to identify vacancies and determine their concentration, but it is also a very sensitive and direct tool for investigating vacancy-solute-atom complexes, since PAS provides specific microstructural (atomistic) information, i.e. characterizing the local chemical surroundings of vacancies [21,22]. This cannot be obtained either by other integral methods such as Vickers micro hardness, differential scanning calorimetry or electrical resistometry, which just provide information about macroscopic properties, nor by imaging methods, e.g. transmission electron microscopy or atom probe tomography, which are insensitive to vacancies and their complexes.

However, studying the interaction between vacancies and solute atoms and determining vacancy-solute atoms binding energies is crucial for improving the microstructure and, thus, the mechanical properties of aluminum alloys in a controlled way. The strength of the interaction between a vacancy and a solute atom can be expressed in terms of their binding energy E_B , which is defined as the difference of the vacancy formation energy in the pure aluminum matrix and in the Al alloy matrix at a nearest neighbor site to the solute atom. Alternatively, this can be seen as a term added to the vacancy migration enthalpy in pure Al altering its magnitude [23,24].

In the past many experimental studies involving other more indirect methods than PAS have been employed to determine the binding energy between vacancies and different solute elements. However, most results do have a wide spread of values or are even contradictory, see for example [25] and Mondolfo Table 1.6 in Chapter 1,2 in [26]. These indirect methods such as electrical resistometry may have been affected by other microstructural processes not detectable by these methods. Furthermore, the purity of the material formerly studied often was either not specified or not high enough to exclude a contribution of unintentional impurities.

Another approach are recent studies calculating the binding energy between vacancies and solute atoms by *ab-initio* methods – see for example [27]. According to *ab-initio* calculations [3,27], the binding energy of vacancies to In and Sn solutes in aluminum

should be in the range of 200–300 meV and, thus, large enough to strongly suppress the decomposition at room temperature. However, even these *ab-initio* calculations are in contradiction to experiments in some cases: e.g. vacancy binding to Mg [28] or Pb [9].

PAS has proven to be a well suited tool for studying the precipitation sequence in binary Al-Cu alloys [29]. Besides our recent work [8,9], there is to the knowledge of the authors only one experimental publication, which studied the interaction of several trace elements with quenched-in vacancies using positron annihilation lifetime spectroscopy (PALS) in a pioneering way [24]. However, the purity of the Al (99.99 %) employed in this study was not as high as in our present work (99.9995 %), i.e. impurity concentrations may be comparable to the concentration of trace elements and, thus, influencing the results. Unfortunately, the decomposition of the measured lifetime spectra has not been shown in [24] – probably due to page limitations in this conference paper.

Recently Francis and Curtin introduced a model for predicting the effectiveness of dilute solutes in delaying precipitate formation employing first principle methods for the calculation of controlling material properties [30]. They found that microalloying, i.e. adding typically a few 100 ppm of solutes, can retard the decomposition process of the alloy and shift the formation of precipitates to a favorable temperature provided that these solutes have sufficiently strong binding energies to vacancies (about 0.2–0.3 eV). The reason is a drastic reduction of the concentration of free vacancies in the lattice after quenching, and thus suppressing the transport of solute atoms. The study [30] predicted that the binding energy of vacancy-solute-atoms is the most important quantity controlling the decomposition kinetics.

In the present work, we used positron lifetime and coincidence Doppler broadening spectroscopies to investigate the thermal evolution of the vacancy-solute-atom interaction in highly diluted Al alloys containing 50 and 250 ppm of In/Sn. Isochronal annealing of the solution heat treated samples was performed to study the thermal evolution of the defects. The binding energy of vacancy-solute complexes was determined in both alloys by isothermal annealing experiments.

The paper is organized as follows: in the following section the details of the experimental work are given. The background of theoretical calculations is introduced in Section 3. Positron lifetime and coincidence Doppler broadening results are presented in Section 4, while Section 5 contains the determination of the binding energies between vacancies and solutes. Section 6 concludes the paper.

2. Experimental details

The alloys studied were prepared by melting very high purity Al (99.9995 %) with In/Sn (99.99 %) in air. Cylindrical rods having 11 mm diameter were cast in a copper mold. The outer most 1 mm of the cylinder was removed to eliminate any probable contamination from the casting process. Thereafter, the alloys were cleaned by ethanol and homogenized for 4 h at 500 °C under the flow of Argon. Slices with thickness of 1 mm were cut to be used for the positron experiments. The samples were subsequently solution heat treated for 2 h at temperatures in the range 320–620 °C. The solution treatment was terminated by a very fast quenching into iced water (0 °C), using a vertical quenching furnace to get the fastest quenching rate. The samples were then moved to the cryostat for lifetime measurements, which started within about 5 min after quenching. During the transfer to the cryostat the sample is 2 min exposed to room temperature. They were isochronally annealed *in-situ* in temperature steps of 10 K up to 337 °C. After each annealing step (holding time 30 min) the samples were cooled down for the lifetime measurements at RT.

A standard temperature-controlled digital positron lifetime spectrometer with a time resolution of 170 ps [8,31] was used in this study.

A 25 μCi ^{22}Na positron-source wrapped in a 6 μm aluminum foil was sandwiched between two identical samples leading to a count rate of 620 c/s. Typically 4.5×10^6 counts were accumulated in each positron lifetime spectrum in about 2 h. A well annealed (550 $^\circ\text{C}$ / 2 h) high purity Al (5N5) was measured as a reference and showed a typical defect-free bulk positron lifetime of 158 ps [8,32] and a source contribution with an intensity of 16.9%, which originates from positron annihilation in the aluminum-foil (160 ps) and the radioactive salt (330 ps) as described in [8]. After source and background corrections, the positron lifetime spectra $n(t) = \sum_{i=1}^{k+1} (I_i/\tau_i) \exp(-t/\tau_i)$ were analyzed by the lifetime program LT9 [33]. One or two exponentially decaying lifetime components convoluted with the Gaussian resolution function of the spectrometer were fitted to the experimental data. The index i stands for the different lifetime components with lifetimes τ_i and their respective intensities I_i . k represents the number of different defect types participating in the positron trapping, which has $k+1$ components in the lifetime spectrum. The presence of vacancy-like defects is indicated by an increase of the average positron lifetime, which is calculated from the decomposed lifetime components according to the formula $\tau_{av} = \sum_{i=1}^{k+1} I_i \tau_i$. This parameter is very sensitive and small changes of its value are accurately detectable [34]. The coincidence Doppler broadening spectroscopy (CDBS) measurements were done using a digital spectrometer in the so-called semi-digital mode, as described in the Refs. [35,36]. The CDBS spectrometer is described in detail in Ref. [29]. The CDBS measurements were carried out at RT and 10^8 counts were accumulated in each spectrum.

3. Theoretical calculations

Density functional theory (DFT) was employed for modelling of vacancies in Al-In and Al-Sn alloys and for the calculations of positron lifetimes and momentum distributions. *Ab-initio* DFT calculations were performed using the plane wave pseudopotential method implemented in the Vienna *ab-initio* Simulation Package (VASP) [37,38]. The projector augmented wave (PAW) [39–41] potentials and the generalized gradient approximation (GGA) with the exchange-correlation functional of Perdew–Burke–Ernzerhof (PBE) [42] were used. The calculations were performed using supercells containing 108 atomic sites and, thus, consisting of $3 \times 3 \times 3$ fcc unit cells with the lattice parameter $a = 4.041$ Å obtained by VASP structure optimization. A reciprocal k -space mesh of $5 \times 5 \times 5$ in the supercell's Brillouin zone and the cut-off energy of 300 eV were used in all calculations. Convergence tests revealed that calculated energies are converged within 0.02 eV.

Vacancies were introduced by removing corresponding atoms from the supercell. Solute impurities were introduced by replacing corresponding Al ions by solute atoms (In or Sn). Equilibrium geometries of all defects were determined by fully relaxing ionic positions in the supercell until the forces on each ion were below 0.01 eV/Å. The vacancy formation energy E_f is calculated from the expression

$$E_f = E_{tot}[V] - \frac{N-1}{N} E_{tot}[\text{bulk}], \quad (1)$$

where $E_{tot}[\text{bulk}]$ and $E_{tot}[V]$ is the total energy of a perfect 108-atom supercell and a supercell containing a vacancy V , respectively, and N is the number of atoms in the perfect supercell. The binding energy E_B of a complex defect consisting of n_V vacancies associated

with n_X solutes ($X = \text{In}$ or Sn) is calculated as

$$E_B = n_V E_{tot}[V] + n_X E_{tot}[X] - E_{tot}[n_V V + n_X X] - (n_V + n_X - 1) E_{tot}[\text{bulk}], \quad (2)$$

where $E_{tot}[n_V V + n_X X]$ is the total energy of a supercell containing a complex defect consisting of n_V vacancies and n_X solutes and $E_{tot}[X]$ is the total energy of a supercell containing solute X . Positive values of the binding energy means attractive interaction between a vacancy and a solute atom, i.e. it is energetically favorable to form vacancy-solute complexes, while negative values of the binding energy means repulsive interaction.

Positron lifetimes were calculated using the so called standard scheme [43], which assumes that the positron density is vanishingly small everywhere and does not affect the bulk electron structure. The electron density $n(\mathbf{r})$ in the material was calculated first without the presence of the positron using the self-consistent valence electron density obtained by VASP with added frozen-core electron densities calculated by a relativistic Dirac-Fock code [44,45]. Subsequently, the effective potential for a positron was constructed as

$$V_+(\mathbf{r}) = \phi(\mathbf{r}) + V_{corr}[n, \nabla n], \quad (3)$$

where $\phi(\mathbf{r})$ is the Coulomb potential produced by the charge distribution of electrons and nuclei and V_{corr} is the electron-positron correlation potential in the limit of vanishing positron density [43]. The ground state of the positron wave function $\psi_+(\mathbf{r})$ and the positron ground state energy eigenvalue E_+ were calculated by solving the single particle Schrödinger equation

$$-\frac{1}{2} \nabla^2 \psi_+(\mathbf{r}) + V_+(\mathbf{r}) \psi_+(\mathbf{r}) = E_+ \psi_+(\mathbf{r}). \quad (4)$$

The solution of the Schrödinger equation was performed on a three-dimensional real space mesh using a finite difference method [46]. The positron lifetime τ was determined by the overlap of the electron density $n(\mathbf{r})$ and the positron density $n_+(\mathbf{r}) = |\psi_+(\mathbf{r})|^2$

$$\tau = \left\{ \pi r_e^2 c \int n_+(\mathbf{r}) n(\mathbf{r}) \gamma[n] d\mathbf{r} \right\}^{-1}, \quad (5)$$

where r_e is the classic electron radius and c is the speed of light. The enhancement in the electron density at the site of the positron due to positron-electron correlation was considered through the enhancement factor γ [43], which was treated within the local density approximation (LDA) using the parametrization by BoronSKI and Nieminen [47]. Calculations of positron lifetimes were performed for non-relaxed defects in the rigid lattice as well as for relaxed geometries of defects in order to observe the effect of ion relaxation on positron lifetime values. The supercell lattice parameter of 4.041 Å obtained from VASP calculations was re-scaled to the experimental value of 4.0495 Å [48] for calculating the positron lifetimes.

The momentum distribution of annihilating electron-positron pairs was calculated using the approach described in Refs. [21,49]. Electrons belonging to a shell of i th atom described by the principal quantum number n and the angular quantum number l contribute to the momentum distribution by

$$\rho^{i,nl}(\mathbf{p}) = 4\pi r_e^2 c N^{i,nl} \gamma^{i,nl} \left| \int R_+^i R_-^{nl} B_l(pr) \mathbf{r}^2 d\mathbf{r} \right|^2, \quad (6)$$

where $N^{i,nl}$ is the number of electrons in the shell, B_l is the spherical Bessel function, and R_+^i and R_-^{nl} denote the radial parts of the positron and electron wave functions, respectively. The symbol $\gamma^{i,nl}$ stands for the state-dependent positron enhancement factor [49]. The total momentum distribution of the annihilating electron-positron pairs was obtained by summing the partial contributions $\rho^{i,nl}(p)$ of the electron shells of all the occupied atomic sites. To account for the finite energy resolution of the CDB spectrometer, the

calculated momentum distributions were convoluted with a Gaussian function having a FWHM of $3.5 \times 10^3 m_0c$. This approach describes well the high momentum part ($p > 10 \times 10^{-3} m_0c$) of the momentum distribution of the annihilating pair with a dominating contribution from core electrons, which retain their atomic character and are almost not affected by crystal bonding. The calculated momentum distributions are presented as ratio curves related to pure Al, which means that the calculated momentum distributions were divided by the momentum distribution calculated for a perfect (defect-free) Al crystal. This enables a comparison of the calculated curves with the results of CDB measurements.

4. Results and discussion

4.1. Positron annihilation lifetime spectroscopy (PALS)

As reference material a high purity 5N5 Al sample has been annealed as described in Section 2 giving a single positron lifetime component (158 ps), which coincides well with earlier reported values [8,29,32]. This sample further serves as a benchmark for the influence of microalloying indium and tin. Hence, it has always been treated under the same solution heat treatment conditions as the In and Sn containing samples.

The average positron lifetime results of the Al-0.025 at% In and the Al-0.025 at% Sn alloys as well as the Al reference material quenched from different solution heat treatment temperatures to iced water are displayed in Fig. 1. In the as-quenched state from 470 and 620 °C the Al reference material showed an average positron lifetime $\tau_{av} = 170$ ps (Fig. 1 (a)) only slightly higher than that of the Al bulk value (158 ps), indicating the formation of just a low concentration of defects surviving the quenching. This is much lower than the average positron lifetime detected in Al-In and Al-Sn samples (230 ps and 240 ps (Fig. 1 (a) and (b)), respectively). We have to note that isolated monovacancies in Al are well known to be mobile at temperatures higher than -50 °C [50,51].

Hence, our observations indicate that In/Sn atoms interact with vacancies forming stable V-In/V-Sn complexes, acting as positron trapping centers. These complexes are thermally stable because they anneal out at higher temperatures in comparison to vacancies in pure Al, indicating that the interaction (and thus the binding

energy) between vacancies and In/Sn atoms is significantly larger than $3/2 kT$ at RT (40 meV).

As shown in Fig. 1 (b), the average lifetime (τ_{av}) of the as-quenched Al-Sn sample increases with increasing solution heat treatment temperature throughout the highest one (620 °C) reaching ~ 240 ps, which can be ascribed to the increase of Sn solubility in the Al matrix [52], while for the Al-In sample τ_{av} increases with increasing solution heat treatment temperature up to 470 °C, where τ_{av} reaches 230 ps. With a further increase of the solution heat treatment temperature, τ_{av} decreases slightly to 220 ps at 620 °C. One obvious possible explanation could be a decreasing In solubility with increasing temperature above 500 °C.

In contrast to tin, to our knowledge, no drawn phase diagram is available for the binary Al-In alloy at low indium content (< 0.03 at.%). However, there are no data supporting the viewpoint of decreasing solubility. Instead according to [53] the solubility of In in Al increases from 0.018 at.% at 530 °C to 0.041 at.% at 638 °C similar to Sn [52].

During isochronal annealing τ_{av} steadily decreases with increasing annealing temperature for samples quenched from temperatures lower than 500 °C. For the lowest temperature before quenching the samples reach the bulk lifetime value fastest. At higher solution heat treatment temperatures ($T > 500$ °C). We find that τ_{av} decreases with the annealing temperature reaching for 127 °C 210 ps (for indium) and 218 ps (for tin). Then τ_{av} increases slightly reaching ~ 220 ps for both In and Sn at an annealing temperature of 170 °C for In and 150 °C for Sn. With further increase of the annealing temperature, τ_{av} decreases again and reaches the bulk level at about 330 °C.

All positron lifetime spectra obtained can be well described by a non-linear fit with two exponentially decaying components. The shorter component with lifetime τ_1 and intensity I_1 represents a contribution of free positrons (not trapped at defects). The longer component with lifetime τ_2 and intensity I_2 is related to positrons trapped at defects. All values are plotted in Fig. 2.

The as-quenched Al reference material showed a defect-related lifetime τ_2 higher than 300 ps with a corresponding intensity $I_2 \sim 12$ % (see upper panel of Fig. 2 (a)). Quenched-in vacancies still migrate during cooling, when some vacancies can meet each other and agglomerate forming vacancy clusters explaining this long positron lifetime. During annealing the defect-related positron lifetime rises to $\tau_2 = 430$ ps at around 100 °C, indicating the formation of even larger vacancy clusters. This signal completely disappears by annealing at temperatures higher than 150 °C.

In contrast, all Al-In or Al-Sn samples, quenched from the different temperatures given above, showed a defect-related positron lifetime $\tau_2 = 247 \pm 3$ ps (In) or 262 ps (Sn), which is for both alloys higher than the lifetime of positrons trapped at Al monovacancies (236 ps), see the calculation below (Table 1). For the indium alloy it is noticeably lower than the characteristic value for a divacancy (257 ps), see the calculations below (Table 1). Hence, both indium and tin atoms bind vacancies forming complexes. Thus, the measured values of τ_2 (247 and 262 ps) are expected to probably correspond to vacancy-In and vacancy-Sn complexes. Their microstructure will be identified in the following.

τ_2 is found to decrease with successive annealing and reaches for 127 °C a minimum value of 230 ± 5 ps for In and 235 ± 5 ps for Sn, which is in good agreement with the calculated lifetime of positrons trapped in a vacancy-solute atom pair (V-In: 233.9 ps / V-Sn: 233.8 ps), i.e. a vacancy associated with an In/Sn solute atom in one of the 12 nearest neighbor sites of the vacancy. Even though, this lifetime value is very close to that of an isolated monovacancy in Al, the tagging to isolated vacancies in Al is not feasible, since they are well known to be mobile at temperatures higher than -50 °C [50,51].

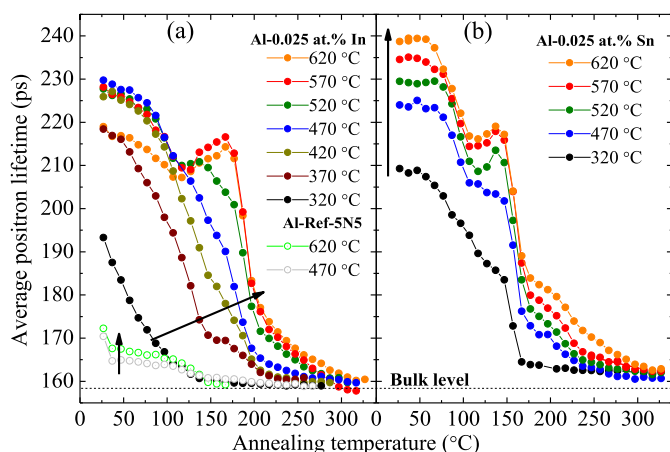


Fig. 1. Average positron lifetime measured in an Al-In (250 ppm) alloy as well as in pure Al after 2 h solution heat treatment at different temperatures in the range 320–620 °C followed by quenching to iced water (a) and an Al-Sn (250 ppm) alloy treated under exactly the same conditions (b). The arrows indicate the direction of increasing solution heat treatment temperature. All measurements were done at RT in between succeeding isochronal annealing steps each lasting 30 min for temperatures up to 337 °C. The average positron lifetime is calculated from the lifetime decomposition presented below in Fig. 2.

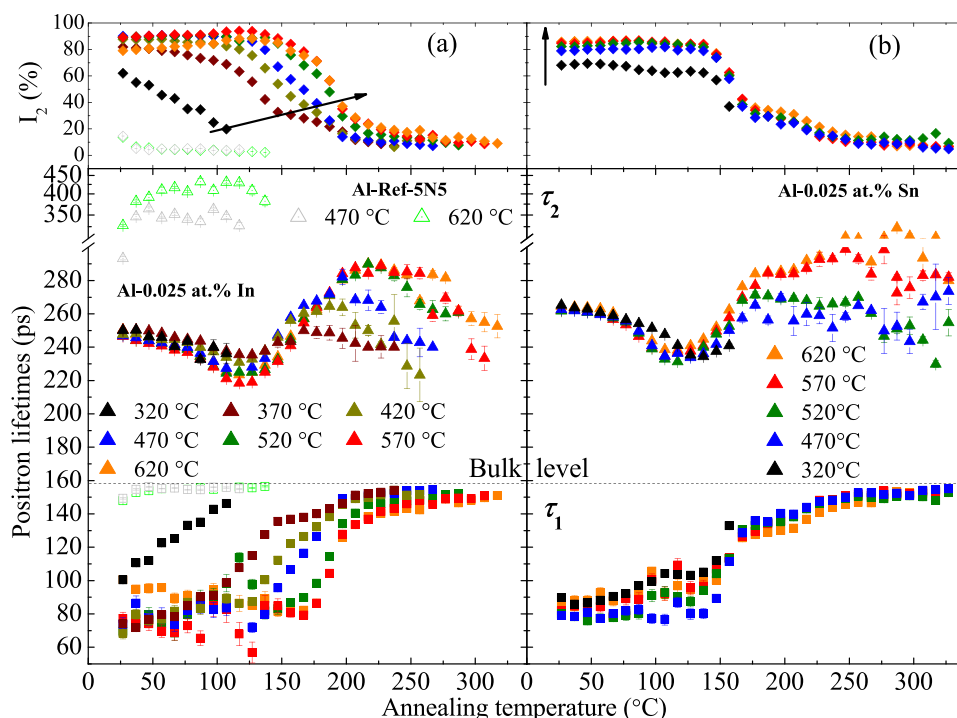


Fig. 2. Results of lifetime spectra decomposition of the Al-0.025 at% In/Sn alloys and a pure Al reference after 2 h solution heat treatment at different temperatures in the range 320–620 °C and then quenched to iced water (a): Al-In and (b): Al-Sn. All measurements were done at RT in between succeeding isochronal annealing steps each lasting 30 min for temperatures up to 337 °C. A 2-component decomposition of the spectra was applied where feasible. The defect-related lifetime τ_2 (triangles) and the reduced bulk lifetime τ_1 (squares) are displayed in the lower panel, while the intensity I_2 (diamonds) related to τ_2 is presented in the upper panel. The arrows show the direction of increasing solution heat treatment temperature.

Since In or Sn solute atoms have larger atomic radii compared to Al ions, an In/Sn atom attached to a vacancy relaxes towards the open space at the vacant atomic site and increases slightly the electron density inside the vacancy, which is reflected as a decrease of the characteristic lifetime of trapped positrons compare to monovacancies in pure Al. With further increase of the annealing temperature, i.e. at $T > 150$ °C, τ_2 is found to increase for both alloys reaching a value of 290–300 ps. This indicates that V-In and V-Sn pairs dissociate, and vacancies freely migrate and, finally, agglomerate forming vacancy clusters.

In the as-quenched state the intensity I_2 of the defect-related positron lifetime component is found to increase slightly with increasing solution heat treatment temperature for Al-In/Al-Sn and pure Al samples. Data for quenching from different solution heat treatment temperatures are presented in the upper panels of Fig. 2. I_2 reaches 90% for 470 °C, i.e. nearly all positrons are trapped. Increasing the solution heat treatment temperatures beyond $T = 500$ °C, I_2 decreases again for Al-In, where one possible explanation could be a limited In solubility, as explained above. Below we will present an alternative explanation in comparison to Al-Sn samples, where this effect is not observed. On isochronal annealing the signal (I_2) related to vacancy-complexes drops faster with decreasing solution heat treatment temperature T for the Al-In alloy compared to the Al-Sn one.

Since the defect-related positron lifetime τ_2 probably is a mixture of contributions from one or several vacancy-solute-atom complexes and vacancy clusters, we have calculated the expected bulk positron lifetime according to the simple trapping model assuming only one kind of defect. All data can be found in Appendix A, while we will present here only the main findings.

For pure Al samples the lifetime τ_1 is very close to the bulk value. The as-quenched samples contain a very low concentration of vacancy clusters: $I_2 \sim 12$ %. For both solution heat treatment

temperatures (470 and 620 °C) the simple trapping model is valid for pure Al, whereas for Al-In samples this is the case only for $T = 320$ °C, when a low amount of thermal vacancies is quenched-in (see Fig. A1). For higher solution heat treatment temperatures (370–620 °C) the Al-In samples show in the as-quenched state a calculated bulk lifetime far from the experimental value of 158 ps. For an increasing annealing temperature at $T > 150 \dots 200$ °C, when I_2 decreases markedly, the calculated bulk lifetime comes close to the experimental value for all solution heat treatment temperatures, which indicates that there is mainly one kind of defect left over.

During the solution heat treatment, most of the thermal vacancies are free because they are continuously attaching and detaching from In / Sn solutes. Vacancy-In / Sn complexes are therefore formed during cooling from the solution treatment temperature. In the course of cooling vacancies are stuck to In / Sn atoms forming V-In / Sn pairs. However, it is possible that some vacancies meet each other instead of meeting In / Sn solutes and agglomerate forming thereby vacancy clusters analogous to what occurs in pure Al. Hence, the Al-In / Al-Sn samples contain most likely vacancy clusters in addition to V-In / Sn pairs.

Ab-initio calculations for vacancy formation and vacancy-solute binding energies as well as of positron lifetimes were employed in order to disclose the nature of defects in the alloys studied. Results of calculations for positrons delocalized in a perfect defect-free lattice (bulk-Al) and positrons trapped in various relaxed and non-relaxed point defects (vacancies and divacancies as well as their complexes with solutes) are listed in Table 1. Our calculated formation energy of an Al monovacancy is 0.55 eV, which agrees well with the value calculated using the PAW GGA potential in Ref. [54] and with other authors employing LDA, e.g. [27], where the value is slightly higher and closer to experiment. As clearly shown in Table 1 in the case of a vacancy associated with one or two

Table 1

Calculated lifetimes of positrons annihilating as free positrons from a delocalized state (bulk-Al) and annihilating from a trapped state in various defects. Results for rigid lattice (non-relaxed) and *ab-initio* relaxed geometry of defects are listed in the table. Displacements of nearest neighbours Al ions in the cases of vacancy / divacancy and vacancy-solute complexes are shown in the table as well. A minus sign in the displacement column means inward relaxation. Binding energies for relaxed configurations of defects are listed in the last column (positive signs mean binding).

defect	non-relaxed τ (ps)	relaxed τ (ps)	displacement (Å)	binding energy (eV)
Bulk-Al	167.6	167.6	-	-
vacancy	244.2	236.3	-0.049	-
divacancy	263.8	256.8	-0.044	-0.10
V-In	241.1	233.9	-0.190	0.23
2V-In	258.9	232.2	-0.662	0.52
2V-2In	254.1	230.0	-0.448	1.03
V-Sn	240.9	233.8	-0.184	0.26
2V-Sn	258.4	233.4	-0.617	0.56
2V-2Sn	253.0	232.0	-0.396	1.11

solute atoms the displacement of these atoms is always negative, meaning an inward relaxation, i.e. towards the unoccupied space in the lattice (vacancy). This effect is observed since all solute atoms considered here (In and Sn) have larger atomic radii than Al.

For a monovacancy the relaxation of solute atoms is simply towards the missing atom (vacancy). In the case of divacancy-solute-atom complexes the relaxation of solutes is basically towards the connecting line between the two vacancies as indicated in Fig. 3. The inward relaxation reduces the positron confinement inside the defect. As a consequence, positron lifetimes calculated for relaxed geometries are shorter compared to those calculated for non-relaxed positions. Moreover, the calculations revealed that vacancies and solute atoms (In or Sn) exhibit an attractive interaction, since the calculated binding energy is positive for all cases. Note that our calculated binding energy for a divacancy in Al is negative (-0.10 eV), in agreement with other calculations Ref. [54]. Hence, a divacancy should be energetically unstable.

Monovacancies having multiple solute atoms as nearest neighbours were considered next. Various crystallographically non-equivalent configurations of n solutes (In or Sn) in nearest neighbor sites around vacancy were considered for each $n = 2, \dots, 12$. Equilibrium configurations of V- n X complexes corresponding to the lowest energy are shown in the appendix (Fig. A2). For example, a V-2X complex consists of solute atoms located in opposite nearest neighbor sites around a vacancy, maximizing the distance between the solutes, see Fig. A2 (a).

Fig. 4 (a) shows the calculated binding energy E_B for V- n In and V- n Sn complexes, i.e. a lowest energy configuration of a single monovacancy surrounded by n In (or Sn) atoms on nearest neighbour sites. One can conclude that the binding energy grows monotonically with the number of solute atoms increasing from

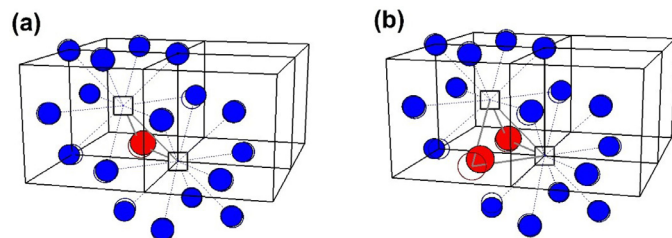


Fig. 3. Schematic depiction of the geometry of 2V-X (a) and 2V-2X (b) complexes, where X denotes the solute (In or Sn). Blue and red circles represent Al and solute atoms, respectively. Open symbols indicate the initial positions in the non-relaxed lattice; full symbols correspond to relaxed positions. Only atoms surrounding vacancies (symbol) in the nearest neighbor sites are shown in the figure.

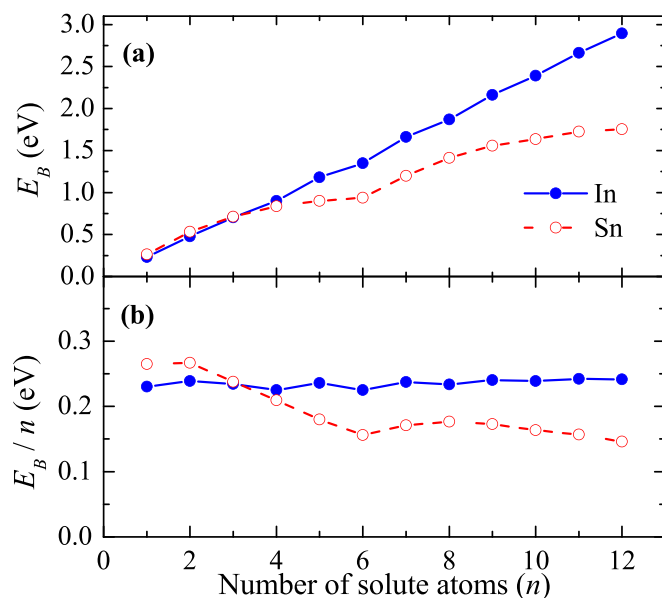


Fig. 4. (a) Calculated binding energy, E_B , for n In or Sn solute atoms as nearest neighbors to a vacancy; (b) The lower part shows the binding energy per solute atom: E_B/n .

$n = 1$ to 12 (12 is the co-ordination number of atomic sites in the fcc lattice). The increase of E_B with the number of solute atoms is nearly linear for In while for Sn E_B gradually saturates for n larger than 6. The binding energy per solute atom, E_B/n , is plotted in Fig. 4 (b). For In solute atoms E_B/n remains nearly constant, while for Sn atoms E_B/n gradually decreases for $n > 2$. Hence, contrary to In solute atoms, binding of additional Sn solute atoms to a V-2Sn complex leads to a lower gain in the binding energy. This indicates that binding of additional Sn atoms to a vacancy becomes weaker due to a repulsive Sn-Sn interaction. Note that since all E_B/n values are positive, V- n X complexes are stable up to $n = 12$. This means that a vacancy surrounded by up to 12 In or Sn solute atoms in nearest neighbor sites has always a lower total energy than an isolated vacancy and the corresponding number of In or Sn solute atoms dissolved randomly in the matrix.

The mean displacement with respect to the centre of the vacant site is plotted for up to 12 indium or tin solute atoms attached to a vacancy in Fig. 5 (a) as a function of their number. For a vacancy surrounded by up to 6 In atoms the displacement of solute atoms is inward (towards the centre of the vacancy). For a higher number of In atoms surrounding the vacancy ($n > 6$) their mutual repulsive interaction prevails and the displacement turns to an outward relaxation, i.e. away from the centre. A similar behaviour was observed for Sn atoms but their displacement turns to an outward relaxation already for $n > 5$, while the magnitude of their displacement is slightly larger. This indicates that the repulsive Sn-Sn interaction is stronger than the corresponding one for In.

Fig. 5 (b) displays calculated characteristic lifetimes for positrons trapped in vacancies surrounded by up to 12 indium or tin solute atoms, where open symbols denote non-relaxed structures while full symbols denote *ab initio* relaxed structures. The positron lifetime values do monotonically decrease with an increasing number of solute atoms for the non-relaxed structures due to the higher electron density of In or Sn atoms. However, a more realistic picture is given by *ab initio* relaxed structures, where the positron lifetime starts to decrease slightly by a few ps with an increasing number of solute atoms around the vacancy. This again reflects a higher electron density at the vacant site due to In/Sn atoms. For a larger number of In/Sn atoms surrounding a

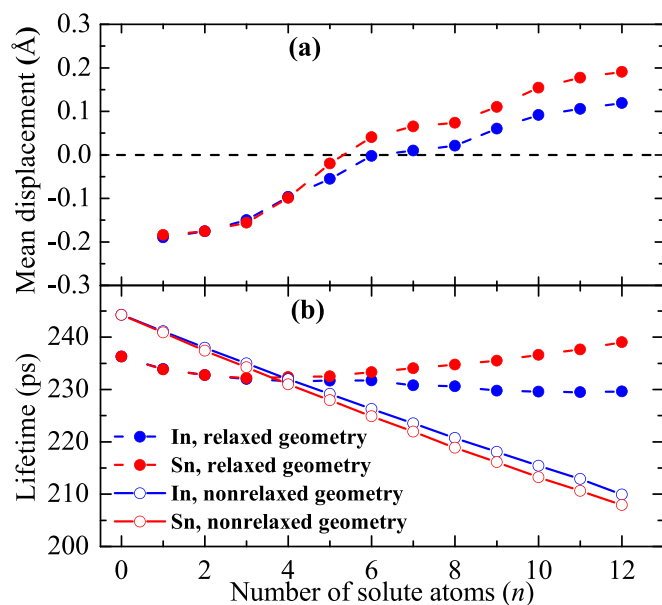


Fig. 5. (a) Mean displacement of solute atoms (In or Sn) surrounding a vacancy; negative (positive) values mean inward (outward) relaxation; (b) Calculated characteristic lifetimes of positrons trapped in vacancy-solute-atom complexes are plotted as a function of the number of solute atoms n surrounding the vacancy, where open symbols represent non-relaxed and full symbols *ab-initio* relaxed structures.

vacancy ($n > 6$ or 5), the characteristic positron lifetime increases due to the outward displacement of Sn atoms as explained above (see Fig. 5 (a)).

Now we compare the calculated positron lifetimes for relaxed defect geometries with experimental results for Al-In alloys in Fig. 2 (a). Obviously, the lifetime τ_2 measured in the as-quenched alloys is a superposition of positrons trapped in vacancies surrounded by one or more In atoms and in vacancy clusters. With increasing annealing temperature vacancy clusters gradually dissolve, where the released vacancies probably attach to In/Sn atoms, and τ_2 decreases to (230 ± 5) ps. This value is close to the calculated lifetimes for positrons trapped in vacancies surrounded by In atoms (see Fig. 5 (b)). Hence, one can conclude that diluted Al-In alloys contain vacancies surrounded by In atoms up to the annealing temperature of 130 °C. At higher temperatures vacancies start to detach from In atoms and the released vacancies either agglomerate forming vacancy clusters or disappear by diffusion to sinks like grain boundaries. Taking into account the experimental uncertainty of ± 5 ps it is not possible to determine the actual number of In/Sn atoms surrounding vacancies solely from the measured positron lifetime. However, the formation of V-In/V-Sn pairs can be considered to be the most likely. It will be shown in the following text that quenched Al-In/Sn alloys indeed contain V-In/V-Sn pairs.

Our results clearly indicated that monovacancies attached to single solute atoms (In or Sn) are responsible for retarding the decomposition of alloys to higher temperatures ($T \geq 150$ °C). Thus, alloys such as Al-Cu and Al-Mg-Si can be micro-alloyed by these elements aiming at increasing the strength of these alloys.

As mentioned above, the diluted Al-In/Sn alloy (250 ppm) in the as-quenched state showed a defect-related positron lifetime of 247 ps or 262 ps, respectively, which is ascribed for both alloys to trapping of positrons at V-In/Sn pairs with an additional contribution of positrons trapped in vacancy clusters. To examine the effect of In/Sn concentration, another Al-In/Sn alloy with a lower In/Sn concentration (50 ppm) was casted and treated under the same thermal conditions: solution heat treatment at 520 °C and quenching to iced water. For all alloys (0.005 and 0.025 at% In/Sn) the positron lifetime decomposition of isochronally annealed sam-

ples is shown in Fig. 6. Clearly the annealing characteristics of the positron lifetime components and their intensities are very similar for both alloys and for the two concentrations. However, we have to note that the defect-related positron lifetime τ_2 is higher for the lower In or Sn concentration: $\tau_2 = 255$ ps (In) or 264 ps (Sn) in the as-quenched state for 50 ppm In/Sn instead of 247/262 ps for 250 ppm In/Sn. For a lower indium/tin concentration the probability for the formation of vacancy clusters should increase in competition to V-In / V-Sn pairs during rapid cooling to 0 °C. Hence, the contribution to τ_2 of vacancy clusters compared with V-In / V-Sn pairs should increase causing the higher value. Since I_2 is very similar for both indium / tin concentrations, obviously a large fraction of the In/Sn atoms in the sample containing 250 ppm In / Sn is not involved in the formation of V-In / V-Sn pairs. During annealing these In/Sn atoms probably form precipitates, which are due to their low number density invisible for PALS.

For the positron trapping coefficient μ only a value for monovacancies in pure Al is reported in the literature: $\mu = 2.5 \times 10^{14} \text{ s}^{-1}$ [55,56]. In Appendix B we show how to derive a more reasonable value for the trapping coefficient in alloys leading to a value of $\mu = 1.5 \times 10^{15} \text{ s}^{-1}$, which should be used.

4.2. Coincidence Doppler broadening spectroscopy (CDBS)

Concerning positron-electron momentum distributions a well-annealed high purity 5N5 Al was used as reference for the ratio curves. The Al-0.005 and Al-0.025 at.% In and Sn samples have been measured at room temperature in the as-quenched state, i.e. solution heat treated at 620 °C and then quenched into iced water. The results of the CDBS measurements are shown in the left part of Figs. 7 and 8, respectively. Our discussion will focus on the high-momentum region $P_L \geq 10 \times 10^{-3} m_0c$ [36,57] because this part of the curves contains the chemical information, i.e. information about the local arrangement of atoms surrounding positron traps.

The ratio curve for a well annealed pure In or Sn sample (shown in the left part of Figs. 7 and 8) shows a similar characteristics as the calculated one (right part). The high momentum part is slightly lower and the low momentum part is higher. This can be ascribed to the existence of a significant amount of vacancies in the pure In sample at RT, i.e. 0.69 of the melting point (156.6 °C). In comparison to In, Sn has a higher melting point (232 °C), thus it contains a significantly lower concentration of thermal vacancies at RT, hence its measured curve is very similar to the calculated one, in particular in the high momentum region. The prominent peak at $P_L = 11 \times 10^{-3} m_0c$ is due to positron annihilation with In- or Sn-4d electrons. Hence, In/Sn atoms surrounding a vacancy, acting as a positron trap, will leave their fingerprint in form of this kind of peak at $P_L = 11 \times 10^{-3} m_0c$ in the CDBS ratio curve.

Calculated CDBS ratio curves for isolated mono- and divacancies as well as for vacancies surrounded by one or two In/Sn atoms are displayed in the right part of Figs. 7 and 8. Evidently, neither isolated mono- nor di-vacancies should exist in the Al-In/Sn alloys, since their characteristics do not fit the experimental data.

The measured curves for both as-quenched Al-In/-Sn samples (50 and 250 ppm In/Sn) show the typical fingerprint of In/Sn as described above (left part of Figs. 7 and 8). We interpret this as the existence of In/Sn atoms surrounding the vacancies. In the low momentum part, the alloy having the smaller In/Sn concentration (50 ppm) is slightly above the alloy with the higher In/Sn concentration (250 ppm). This can be attributed to a higher number of positrons annihilating in vacancy clusters in the alloy with the lower In/Sn content - cf. also PALS data in Fig. 6 (a) and (b).

Similarly to Al-In alloys, the Al-Sn samples can contain neither isolated vacancies nor divacancies because the measured CDBS

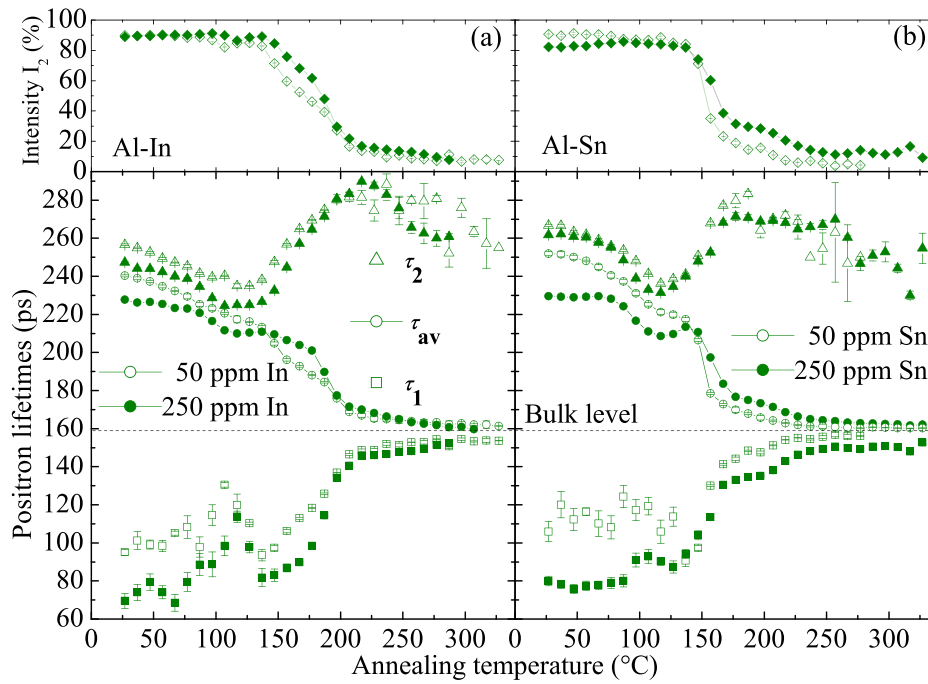


Fig. 6. Al-In and Al-Sn samples (50 and 250 ppm In/Sn) quenched from 520 °C (solution heat treatment temperature) and subsequently isochronally annealed at the given temperature. The lifetime decomposition τ_1 and τ_2 as well as τ_{av} are shown in the lower panel and the intensity I_2 of the defect-related lifetime is presented in the upper panel. Concerning Al-0.025 at.% In/Sn the data are the same as in Fig. 2.

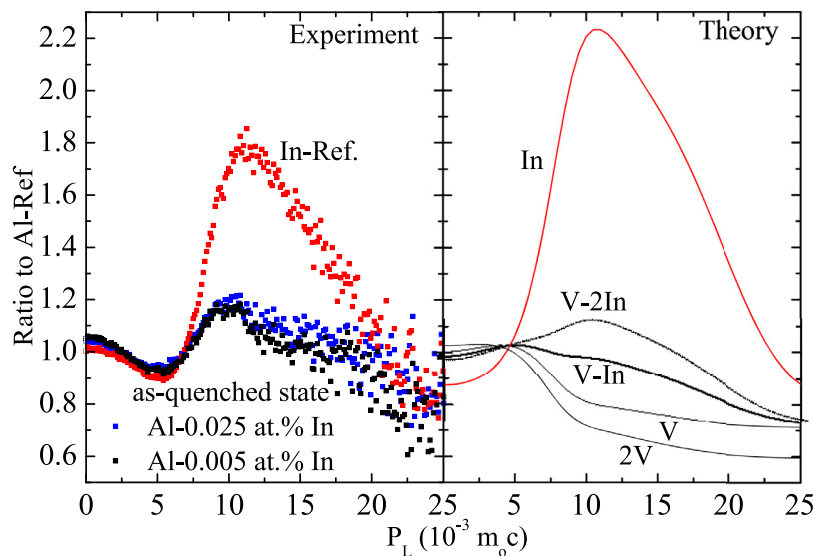


Fig. 7. Momentum distribution of the annihilating electron-positron pairs with respect to the 5N5 Al bulk reference sample. The left panel shows spectra of the Al-In alloy (0.005 and 0.025 at.% In) as well as the spectrum of the pure indium reference. The samples were solution heat treated for 2 h at 620 °C, then quenched into iced water, and finally measured by CDBS at RT. The right panel displays calculated ratio curves with respect to Al for mono- and di-vacancies as well as for vacancy-In complexes in relaxed geometry.

curves contain clear contributions of positrons annihilated in the vicinity of Sn.

In the high momentum region the measured CDBS ratio curves are slightly above the calculated one for the V-In/V-Sn complexes and below the curve for V-2In/V-2Sn complexes, indicating that the defect observed in the as-quenched Al-In/Al-Sn alloys is probably a mixture of both. However, the binding energy determined below is very close to the calculated one for V-In/V-Sn and much lower than that of V-2In/V-2Sn complexes, suggesting that the predominating defects are V-In/V-Sn complexes.

Fig. 9 (a) and (b) shows the CDBS ratio curves measured for the Al-0.025 at.% In and Sn alloys, respectively, solution heat treated

at 620 °C, quenched to iced water and then annealed at different temperatures. All measured spectra show the fingerprint due to 4-d electrons of In/Sn, and thus In/Sn atoms are supposed to be (nearest) neighbours to vacancies. It is important to note that the ratio curve of the sample annealed at 127 °C is distinctly higher than that of the as-quenched sample, which can be ascribed to the existence of mainly V-In or V-Sn pairs in the sample after this annealing step, i.e. vacancy clusters forming during rapid cooling have completely recovered. In addition, there may be probably some In/Sn agglomerates in the samples, which increase the In contribution to the CDBS curves. This results in the highest ratio (1.4 or 1.2) and the shortest τ_2 (220 or 230 ps) for (In or Sn) in the sam-

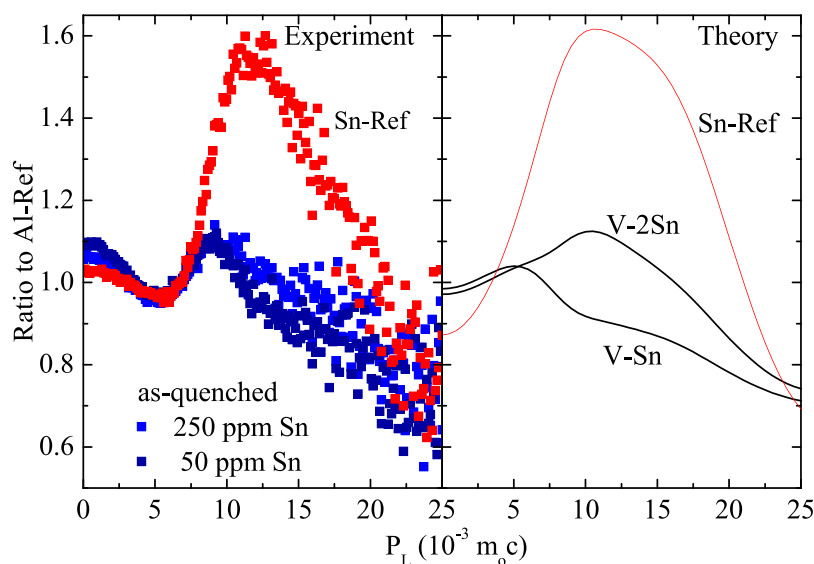


Fig. 8. CDBS ratio curves with respect to Al measured in the Al-0.005 and 0.025 at.% Sn alloys as well as in the pure tin reference sample and normalized to the Al bulk (left part). Treatment as described in Fig. 7. The right panel displays the theoretically calculated CDBS ratio curves for different vacancy-Sn complexes and pure Sn in relaxed geometry. The momentum distribution corresponding to vacancies attached to Sn atoms (V-Sn solutes) is in good agreement with the measured curve of the as-quenched Al-Sn alloy.

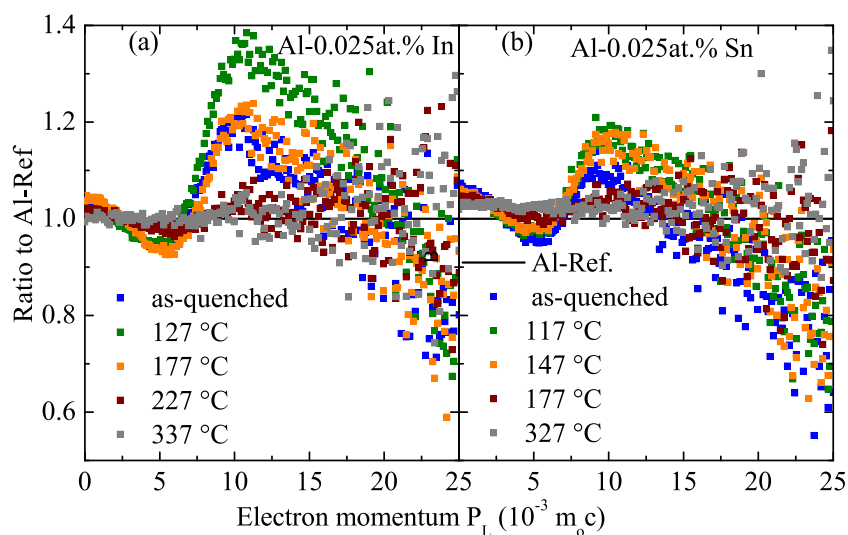


Fig. 9. CDBS ratio curves with respect to pure Al for the Al-0.025 at.% In/Sn alloys (a)/(b) after solution heat treatment at 620 °C, quenching to iced water and annealing at different temperatures. CDBS measurements were performed at RT between successive isochronal annealing steps. The In or Sn fingerprint is most distinct for annealing at 127 °C. Then it fades out reaching nearly the bulk level after annealing at 337 °C.

ple solution heat treated at 620 °C. The In/Sn fingerprint in the CDBS ratio curve fades out with further annealing ($T = 177$ and 227 °C). It almost reaches the bulk level after annealing at 337 °C. This occurs due to the dissociation of V-In/V-Sn complexes and agglomeration of released vacancies into vacancy clusters. However, some In or Sn atoms remain in solution in the matrix and its signal is visible in the CDBS ratio curves even after annealing at the highest temperature (337 °C), where the CDBS curve is very close to, but slightly above the Al reference sample for high momenta.

It is noteworthy that there is only a very small difference of positron annihilation parameters (CDBS curves, lifetime τ_2 , intensity I_2) for Al-In/Al-Sn alloys containing 50 and 250 ppm In/Sn although the difference in the In/Sn concentration between the different alloys is large (1:5). This shows that a large fraction of In or Sn in the 250 ppm samples is not actually participating in the formation of V-In/V-Sn pairs. This is expected due to the much

lower concentration of quenched-in vacancies compared to 50 ppm solute atoms. Hence, a large fraction of In or Sn is present in the sample in solution or as agglomerates (clusters/precipitations), which could in principle act as additional traps for positrons. However, their number density can be estimated too low to be detectable. The increase of the CDBS ratio curve (to 1.4 for In and 1.2 for Sn - see Fig. 7) measured in Al-In and Al-Sn sample with 50 ppm content annealed at 127 °C may be due to non-existing competition trapping to vacancy cluster anymore.

5. Determination of the binding energy of vacancy-solute atoms

The vacancy-solute-atom binding energy reflects how strong vacancies are bound to solute atoms. Consequently, a determination of the binding energy is fundamental to understand the interaction between the solute atoms and vacancies.

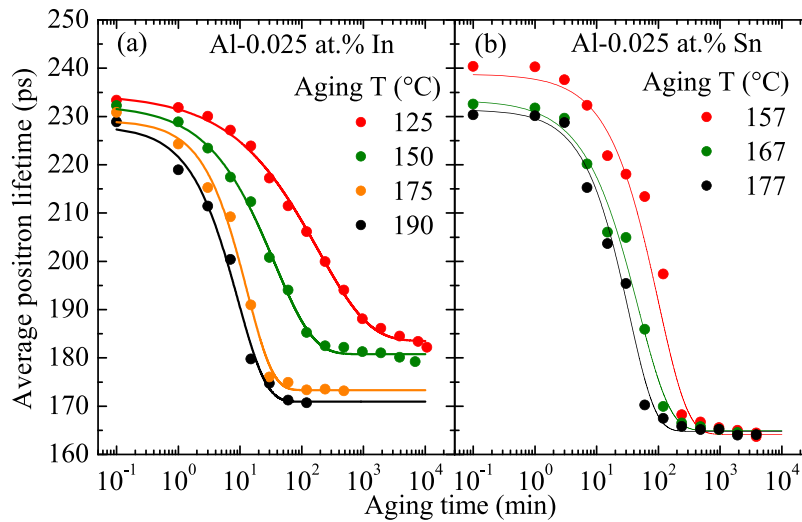


Fig. 10. Isothermal annealing curves of the average positron lifetime for Al-0.025 at.% In/Sn alloys annealed at 125, 150, 175, and 190 °C for In (a) and at 157, 167, and 177 °C for Sn (b) after quenching the samples from 420 °C into iced water. Solid lines are model curves calculated by Eq. (7).

In the present study we use highly pure Al 99.9995% and employ the well-known cross-cut of curves method [58,59] for determining the activation energy of defect migration via isothermal annealing.

The quenched Al-0.025 at.% In sample was isothermally annealed at 125, 150, 175, and 190 °C, while the Al-Sn alloy was thermally annealed at 157, 167, and 177 °C. The evolution of the average positron lifetime as a function of aging time during isothermal annealing is plotted in Fig. 10. The average positron lifetime decreases with increasing annealing time since vacancies recover by migration to sinks like grain boundaries. The recovery of vacancies is a thermally activated process and proceeds faster at higher temperatures, which is reflected by a faster decrease of the average positron lifetime. Isothermal curves of the average positron lifetime can be described by the expression

$$\tau_{av} = a(1 - \exp(-t/\tau_r)^m) + b, \quad (7)$$

i.e. using the well-known Kolmogorov-Johnson-Mehl-Avrami equation [60–62] modified for the description of the average positron lifetime curves by multiplying it by a (negative) scaling constant a and adding a constant factor b . The parameter τ_r is a characteristic time scale for the recovery of vacancies (it is the time period necessary for a decrease of the vacancy concentration to $1 - e^{-1} = 0.63$ fraction of its initial value) and m is the Avrami coefficient [62]. Model curves calculated by Eq. (7) are plotted in Fig. 10 (a) and (b) (solid lines) for Al-In and Al-Sn, respectively, and one can see that experimental curves of the average positron lifetime are described by Eq. (7) very accurately. The Avrami coefficient m obtained from the fitting fell into the range from 0.5 to 1.0.

Since the recovery of vacancies is a thermally activated process, the rate of this process is governed by the Arrhenius equation

$$\tau_r^{-1} = A \exp(-E_a/k_B T) \quad (8)$$

where k_B is the Boltzmann constant, T is absolute temperature of isothermal annealing, and E_a is the activation energy for the recovery of vacancies. Applying the logarithm on Eq. (8) one obtains the relation

$$\ln \tau_r = \frac{E_a}{k_B T} + \ln A. \quad (9)$$

Hence, the activation energy E_a can be determined from an Arrhenius plot, i.e. by plotting $\ln \tau_r$ versus $1/k_B T$. Providing that the above assumptions are correct, the Arrhenius plot should be a straight line with the slope E_a . As shown in Fig. 11 (a) and (b)

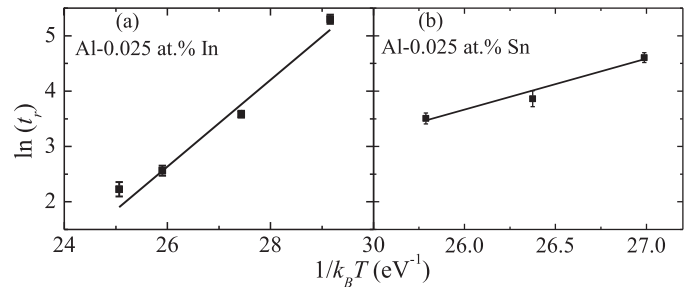


Fig. 11. Arrhenius plots of the characteristic vacancy recovery period τ_r for the Al-0.025 at.% In/Sn samples isothermally annealed at different temperatures shown in Fig. 10 (a) and (b). The solid line represents a linear fit to the experimental data giving an activation energy $E_a = (0.78 \pm 0.03)$ eV for the Al-In alloy and (0.90 ± 0.10) eV for the migrating V-Sn pairs.

this is indeed the fact for our data taking into account experimental uncertainties. Fitting yields a slope (E_a) of (0.78 ± 0.03) and (0.90 ± 0.10) eV for migrating of V-In and V-Sn pairs, respectively. Since vacancies are associated with In/Sn solute atoms the derived activation energy E_a is the sum of the vacancy migration energy E_M and the binding energy E_B of vacancies to solute-atoms, i.e. $E_a = E_M + E_B$, because vacancies have to be released from In/Sn-atoms and they have to move (jump) through the potential well between atomic sites. Using the vacancy migration energy in Al $E_M = (0.58 \pm 0.03)$ eV determined in Ref. [63], one obtains the binding energy of vacancy to In solute atoms $E_B = (0.20 \pm 0.03)$ eV and for Sn solute atoms $E_B = (0.32 \pm 0.10)$ eV. This agrees well with our calculated value in Table 1 and the result of Hutchinson [24] (0.19 eV for indium and 0.25 eV for tin) as well as results of theoretical calculations in Refs. [3,27].

Table 2 summarizes the binding energies for vacancy-solute-atom pairs determined experimentally in our work comparing them to *ab-initio* calculations reported by Wolverton [27] and Peng et al. [3] and to other experimental work. One can conclude that vacancy-solute binding energies determined in the present experiment are in good agreement with the *ab-initio* theoretical calculations and fall into the range of most older experimental data.

However, the uncertainties in values for vacancy-solute-atom binding energies determined by PALS measurements in Ref. [24] can most likely attributed to the impurities of the formerly used alloys and/or the positron trapping coefficient.

Table 2

Binding energies of vacancies to In and Sn solute atoms determined experimentally in this work in comparison to the values obtained by *ab-initio* calculations and other experiments.

Solute	Binding energy (eV)				
	Theory [3,27]	Theory (this work)	Experiment (this work)	Experiment [24]	Exp. Data [26]
In	0.20	0.23	0.20 ± 0.03	0.19	0.19 ... 0.42
Sn	0.25	0.26	0.32 ± 0.10	0.25	0.22 ... 0.46

6. Conclusion

In summary, we employed positron annihilation spectroscopy using both positron lifetime and coincidence Doppler broadening spectroscopies for studying the interaction between vacancies and solute-atoms in high purity 5N5 aluminum micro-alloyed with indium and tin (50 and 250 atomic ppm). Our comprehensive positron annihilation study was accompanied by state-of-the-art *ab-initio* DFT theoretical calculations on vacancy formation energies and on vacancy-solute-atom binding energies. From the obtained results one can conclude that there is a significant attractive interaction between vacancies and In or Sn solute-atoms being very similar. However, we obtain accurate vacancy-solute-atom binding energies.

During solution heat treatment, nearly all thermal vacancies are free because they are continuously attaching and detaching from In or Sn atoms in solid solution. Stable vacancy-In/Sn complexes are supposed to be formed during rapid cooling from the solution heat treatment temperature. In the course of cooling vacancies stick to In or Sn atoms forming V-In/V-Sn pairs. However, it is possible that some vacancies meet each other instead of meeting In or Sn solute atoms and, thus, they agglomerate forming vacancy clusters.

Also in a high purity Al reference sample subjected to a solution heat treatment at 620 and 470 °C followed by quenching to iced water a weak signal from vacancy clusters was observed. Those vacancy clusters were obviously formed by agglomeration of quenched-in vacancies during rapid cooling of the Al sample.

However, the CDBS investigations confirmed that in the as-quenched state most of the observed defects in Al-In and Al-Sn alloys indeed are vacancies attached to solute atoms (V-In/V-Sn pairs).

Smaller, less stable vacancy clusters formed during rapid cooling are found to anneal out in the temperature range up to 130 °C, while vacancy-solute-atom pairs are thermally stable up to about 150 °C. A further increase of the annealing temperature causes the dissociation of the vacancy-solute complexes. The released vacancies agglomerate forming larger, more stable vacancy clusters, which are eventually annealed out at about 300 °C.

Employing isothermal annealing of quenched alloys binding energies of (0.20 ± 0.03) eV and (0.32 ± 0.10) eV were experimentally determined for vacancies attached to In and Sn solute-atoms, respectively. These values are in excellent agreement with results of *ab-initio* DFT calculations [3,27] and other experimental studies [24,26] and are also in accordance with the microalloying model [30] introduced for controlling of material properties.

Important for alloy design is the knowledge that quenched-in vacancies are bound to these solute-atoms forming V-In and V-Sn pairs, which are stable up to 150 °C. At higher temperatures the vacancy-solute pairs dissociate, and vacancies are released. Consequently, In or Sn is added to Al alloys (e.g. age hardenable alloys such as Al-Cu) to preserve (or store) the quenched-in vacancies, suppressing GP-I and GP-II / Θ' formation, and then release them at the temperature of the Θ' formation enhancing the diffusion of Cu atoms.

Thus, our work reduces the uncertainties in values for vacancy-solute-atom binding energies by direct identification of the atomic

species involved. In the future more such research is needed to put modern alloy design by microalloying addition on a firm basis.

Declaration of Competing Interest

The authors declare that they have no known competing financial interests or personal relationships that could have appeared to influence the work reported in this paper.

Acknowledgments

This work is supported by the German Research Foundation DFG (KR-1269/24-1 and STA-527/5-1). Computational resources for DFT calculations were supplied by the project "e-Infrastruktur CZ" (e-INFRA LM2018140) provided within the program Projects of Large Research, Development and Innovations Infrastructures.

Appendix A

A. Validity of the trapping model

To check the validity of the two-state simple trapping model [20], the bulk lifetime is calculated from the lifetime decomposition for the samples presented in Fig. 2 using the equation:

$$\tau_b = \left(\frac{I_1}{\tau_1} + \frac{I_2}{\tau_2} \right)^{-1} \quad (\text{A1})$$

where τ_i and I_i stand for the lifetime and its corresponding intensity of each component, the results are shown in Fig. A1. The pure Al sample shows calculated bulk lifetime values very close to the experimental value of 158 ps, indicating the validity of the

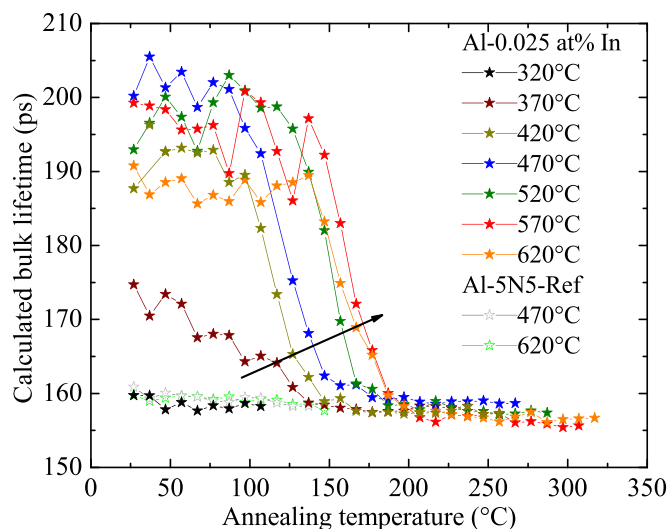


Fig. A1. Bulk lifetimes calculated from the lifetime spectra decomposition in Fig. 2 (a) by applying the two-state simple trapping model (Eq. (A1)). The large difference between calculated and measured bulk lifetimes in Al-In samples is obvious, suggesting that the samples contain two different kinds of defects (traps).

two-state trapping model, i.e. the presence of only one trap (defect type) throughout the whole annealing. The detected traps are identified as vacancy clusters.

In contrast, all Al-In samples quenched from temperatures at 370 °C and above showed calculated bulk lifetime values according to Eq. (A1) much higher than 158 ps. This indicates the existence of more than one defect type in these samples, which reveals that the second lifetime component is likely a superposition of positron trapping at two different trapping centers. The calculated values reach the bulk level with annealing the samples earlier when the solution heat treatment temperature decreases. The value calculated for sample solution heat treated at 370 °C reaches the bulk after annealing at 130 °C but for the sample solution heat treated at 620 °C it reaches the bulk after annealing at 180 °C. The lower the solution heat treatment temperature is, the faster the calculated bulk lifetime reaches the measured value. This is caused most probably by the fact that the concentration of thermal vacan-

cies and thereby also the size of vacancy clusters formed during quenching is smaller in samples solution treated at lower temperatures.

As mentioned above, the pure Al samples showed the presence of vacancy clusters, with a lifetime varying in the range from 300 to 430 ps and an intensity decreasing from 12 to 0 % over the annealing. Therefore, the component of the vacancy clusters in Al-In / Al-Sn alloys is very difficult to be decomposed or even fixed because its lifetime value is altering and its intensity is noticeably low. Thus, the second lifetime component τ_2 corresponds to positron annihilation in both defects, vacancy-solute complexes and vacancy clusters in quenched alloys.

Fig. A2 shows the structure of different V-nX complexes ($X = \text{In}$ or Sn, $n = 2, \dots, 12$) obtained from *ab-initio* calculations. Open circles show initial positions in the non-relaxed lattice, while full circles represent relaxed positions for In solutes.

Appendix B

B. Determination of the trapping coefficient for vacancies in solid solutions

For the positron trapping coefficient μ only a value for mono-vacancies in pure Al is reported in the literature: $\mu = 2.5 \times 10^{14} \text{ s}^{-1}$ [55,56]. However, the positron trapping rate to vacancies can be expressed within the simple trapping model using the relation

$$\kappa = \mu C = \frac{1}{\tau_b} \frac{\tau_{av} - \tau_b}{\tau_d - \tau_{av}} \quad (\text{B1})$$

where τ_b is the bulk lifetime of 158 ps, τ_{av} is the average lifetime, $\tau_d = \tau_2$ is the defect-related positron lifetime, where we assume 233.9 ps for V-In solutes according to our *ab-initio* calculations. The concentration C of thermal vacancies in Al at a temperature T is given by the equation

$$C = \exp(S/k_B) \exp(-E_F/k_B T) \quad (\text{B2})$$

where k_B is the Boltzmann constant, $E_F = 0.67 \text{ eV}$ is the most probable experimental value of vacancy formation energy in Al [64] and $S = 0.7k_B$ is a typical value of the vacancy formation entropy in metals [64]. Using the concentration of thermal vacancies at the solution heat treatment temperature expressed by Eq. (B2) and inserting it into Eq. (B1), one can calculate the average positron life-

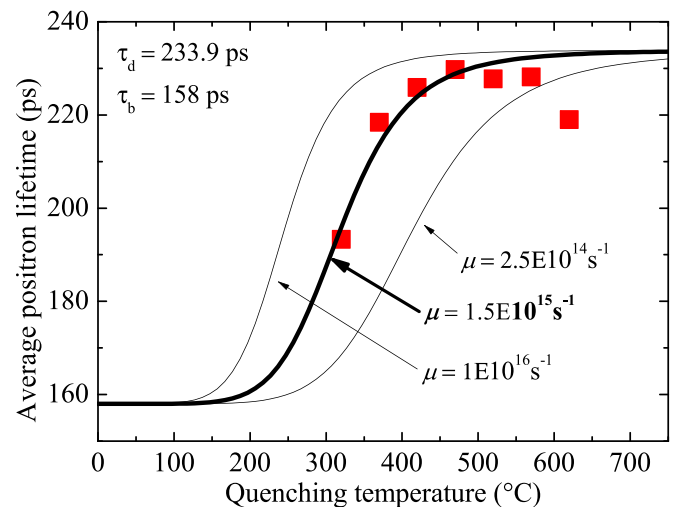


Fig. B1. Average positron lifetimes calculated using different values of the specific trapping rate μ (solid lines) compared to experimental data (red squares) measured immediately after quenching for various solution heat treatment temperatures (data as in Fig. 1 (a)). The best agreement with experimental data was obtained for a trapping coefficient $\mu = 1.5 \pm 1 \times 10^{15} \text{ s}^{-1}$.

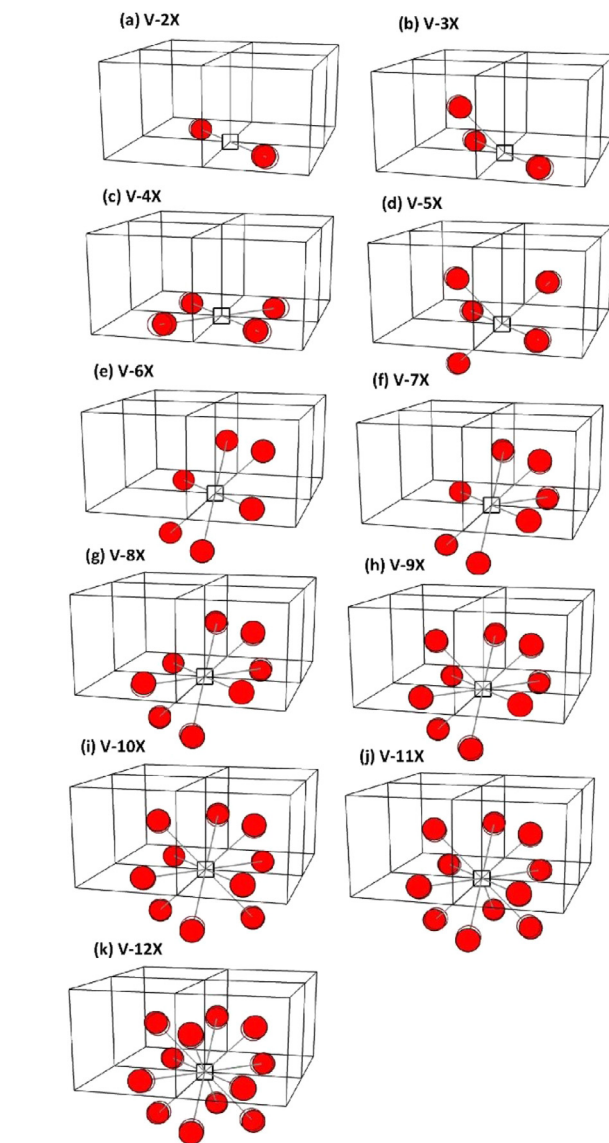


Fig. A2. Geometries of lowest energy configurations of V-nX complexes ($X = \text{In}$ or Sn, $n = 2, \dots, 12$) obtained from *ab-initio* calculations. Only the vacancy (denoted by a square) and solute atoms (In or Sn) are shown. Open circles indicate initial (ideal) positions in the non-relaxed lattice, full circles correspond to relaxed (real) positions for In solutes (displacements of Sn solutes are similar but slightly higher in magnitude).

time from Eq. (B1) and compare it with experimental values. Results presented in Fig. B1 clearly show that the average positron lifetime curve calculated using the trapping coefficient for mono-vacancies $\mu = 2.5 \times 10^{14} \text{ s}^{-1}$ does not match the experimental data well. However, the best agreement with experiment was obtained employing a trapping coefficient $\mu = 1.5 \times 10^{15} \text{ s}^{-1}$, which should be, therefore, applied for calculating of the defect concentration.

References

- [1] F. Ostermann, *Anwendungstechnologie Aluminium*, 3rd ed., Springer-Verlag, Berlin, 2014.
- [2] W. Sun, Y. Zhu, R. Marceau, L. Wang, Q. Zhang, X. Gao, C. Hutchinson, Precipitation strengthening of aluminum alloys by room-temperature cyclic plasticity, *Science* 363 (2019) 972–975, doi:10.1126/science.aav7086.
- [3] J. Peng, S. Bahl, A. Shyam, J.A. Haynes, D. Shin, Solute-vacancy clustering in aluminum, *Acta Mater.* 196 (2020) 747–758, doi:10.1016/j.actamat.2020.06.062.
- [4] D. Shin, A. Shyam, S. Lee, Y. Yamamoto, J.A. Haynes, Solute segregation at the Al/ θ' -Al₂Cu interface in Al-Cu alloys, *Acta Mater.* 141 (2017) 327–340, doi:10.1016/j.actamat.2017.09.020.
- [5] I. Poon, R.K.W. Marceau, J. Xia, X.Z. Liao, S.P. Ringer, Precipitation processes in Al-Cu-Mg-Sn and Al-Cu-Mg-Sn-Ag, *Mater. Des.* 96 (2016) 385–391, doi:10.1016/j.matdes.2016.02.048.
- [6] J.M. Silcock, T.J. Heal, H.K. Hardy, The structural ageing characteristics of ternary aluminium-copper alloys with cadmium, indium, or tin, *J. Inst. Met.* 84 (1955) 23.
- [7] J.M. Silcock, T.J. Heal, H.K. Hardy, Intermediate precipitates in aged binary alloys of aluminium with cadmium, indium or tin, *J. Inst. Metal.* 84 (1955) 19–22.
- [8] F. Lotter, U. Muehle, M. Elsayed, A.M. Ibrahim, T. Schubert, R. Krause-Rehberg, B. Kieback, T.E.M. Staab, Precipitation behavior in high-purity aluminium alloys with trace elements – the role of quenched-in vacancies, *Phys. Status Solidi A Appl. Mater. Sci.* 215 (2018) 1–11, doi:10.1002/pssa.201800375.
- [9] T.E.M. Staab, F. Lotter, U. Muehle, M. Elsayed, D. Petschke, T. Schubert, A.M. Ibrahim, R. Krause-Rehberg, B. Kieback, The decomposition process in high-purity Al-1.7 at.% Cu alloys with trace elements: preservation of quenched-in vacancies by In, Sn and Pb influencing the θ' formation, *J. Mater. Sci.* 56 (2021) 8717–8731, doi:10.1007/s10853-020-05742-9.
- [10] F. Lotter, D. Petschke, F. De Geuser, M. Elsayed, G. SEXTL, T.E.M. Staab, *In situ* natural ageing of Al-Cu(Mg) alloys: the effect of In and Sn on the very early stages of decomposition, *Scr. Mater.* 168 (2019) 104–107, doi:10.1016/j.scriptamat.2019.04.031.
- [11] C.R. Hutchinson, P.T. Loo, T.J. Bastow, A.J. Hill, J. da Costa Teixeira, Quantifying the strain-induced dissolution of precipitates in Al alloy microstructures using nuclear magnetic resonance, *Acta Mater.* 57 (2009) 5645–5653, doi:10.1016/j.actamat.2009.07.060.
- [12] Y. Zhang, Z. Zhang, N.V. Medhekar, L. Bourgeois, Vacancy-tuned precipitation pathways in Al-1.7 Cu-0.025In-0.025Sb (at.%) alloy, *Acta Mater.* 141 (2017) 341–351, doi:10.1016/j.actamat.2017.09.025.
- [13] F. Lotter, D. Petschke, T.E.M. Staab, U. Rohrmann, T. Schubert, G. SEXTL, B. Kieback, The influence of trace elements (In, Sn) on the hardening process of Al-Cu alloys, *Phys. Status Solid A* 215 (2018) 1800038, doi:10.1002/pssa.201800038.
- [14] M. Liu, X. Zhang, B. Körner, M. Elsayed, Z. Liang, D. Leyvraz, J. Banhart, Effect of Sn and In on the natural ageing kinetics of Al-Mg-Si alloys, *Materialia* 6 (2019) 100261, doi:10.1016/j.mta.2019.100261.
- [15] W. Tu, J. Tang, Y. Zhang, L. Ye, S. Liu, J. Lu, X. Zhan, C. Li, Effect of Sn and Cu addition on the precipitation and hardening behavior of Al-1.0Mg-0.6Si alloy, *Mater. Sci. Eng. A* 770 (2020) 138515, doi:10.1016/j.msea.2019.138515.
- [16] S. Pogatscher, H. Antrekowitsch, M. Werinos, F. Moszner, S.S.A. Gerstl, M.F. Francis, W.A. Curtin, J.F. Löffler, P.J. Uggowitzer, Diffusion on demand to control precipitation aging: application to Al-Mg-Si alloys, *Phys. Rev. Lett.* 112 (2014) 225701, doi:10.1103/PhysRevLett.112.225701.
- [17] S. Pogatscher, M. Werinos, H. Antrekowitsch, P.J. Uggowitzer, The role of vacancies in the aging of Al-Mg-Si alloys, *Mater. Sci. Forum* 794–796 (2014) 1008–1013, doi:10.4028/www.scientific.net/MSF.794-796.1008.
- [18] M. Werinos, H. Antrekowitsch, T. Ebner, R. Prillhofer, W.A. Curtin, P.J. Uggowitzer, S. Pogatscher, Design strategy for controlled natural aging in Al-Mg-Si alloys, *Acta Mater.* 118 (2016) 296–305, doi:10.1016/j.actamat.2016.07.048.
- [19] P. Heitjans, J. Kärger, *Diffusion in Condensed Matter: Methods, Materials, Models*, Springer Science & Business Media, 2006.
- [20] R. Krause-Rehberg, H.S. Leipner, *Positron Annihilation in Semiconductors: Defect Studies*, Springer Science & Business Media, Berlin, 1999.
- [21] M. Alatalo, B. Barbiellini, M. Hakala, H. Kauppinen, T. Korhonen, M.J. Puska, K. Saarinen, P. Hautojärvi, R.M. Nieminen, Theoretical and experimental study of positron annihilation with core electrons in solids, *Phys. Rev. B* 54 (1996) 2397–2409, doi:10.1103/PhysRevB.54.2397.
- [22] P. Asoka-Kumar, M. Alatalo, V.J. Ghosh, A.C. Kruseman, B. Nielsen, K.G. Lynn, Increased elemental specificity of positron annihilation spectra, *Phys. Rev. Lett.* 77 (1996) 2097–2100, doi:10.1103/PhysRevLett.77.2097.
- [23] M. Doyama, Vacancy-solute interactions in metals, *J. Nucl. Mater.* 69–70 (1978) 350–361, doi:10.1016/0022-3115(78)90253-2.
- [24] C. Hutchinson, B.M. Gable, N. Ciccosillo, P. Loo, T.J. Bastow, A.J. Hill, An experimental determination of solute-vacancy binding energies in high purity dilute Al-X alloys, in: *Proceedings of the International Conference on Aluminium Alloys (ICAA)*, Wiley-VCH Verlag GmbH & Co. KGaA, 2008, pp. 788–794.
- [25] O. Melikhova, J. Kuriplach, J. Čížek, I. Procházka, Vacancy-solute complexes in aluminum, *Appl. Surf. Sci.* 252 (2006) 3285–3289, doi:10.1016/j.apsusc.2005.08.052.
- [26] L.F. Mondolfo, Structure, in: L.F.B.T.-A.A. Mondolfo (Ed.), *Aluminum Alloys: Structure and Properties*, Butterworth-Heinemann, 1976, pp. 11–55, doi:10.1016/B978-0-408-70932-3.50008-5.
- [27] C. Wolverton, Solute-vacancy binding in aluminum, *Acta Mater.* 55 (2007) 5867–5872, doi:10.1016/j.actamat.2007.06.039.
- [28] M. Liu, B. Klobes, J. Banhart, Positron lifetime study of the formation of vacancy clusters and dislocations in quenched Al, Al-Mg and Al-Si alloys, *J. Mater. Sci.* 51 (2016) 7754–7767.
- [29] M. Elsayed, A.M. Ibrahim, T.E.M. Staab, R. Krause-Rehberg, A new perspective on the precipitation sequence in a high-purity Al-1.74at.%Cu alloy by employing positron annihilation spectroscopy: experiment and theory, *J. Phys. Condens. Matter* (2021) <http://iopscience.iop.org/article/10.1088/1361-648X/ac17af>.
- [30] M.F. Francis, W.A. Curtin, Microalloying for the controllable delay of precipitate formation in metal alloys, *Acta Mater.* 106 (2016) 117–128, doi:10.1016/j.actamat.2016.01.014.
- [31] O. Hauenstein, M.M. Rahman, M. Elsayed, R. Krause-Rehberg, S. Agarwal, V. Abetz, A. Greiner, Biobased polycarbonate as a gas separation membrane and “breathing glass” for energy saving applications, *Adv. Mater. Technol.* 2 (2017), doi:10.1002/admt.201700026.
- [32] T.E.M. Staab, E. Zschech, R. Krause-Rehberg, Positron lifetime measurements for characterization of nano-structural changes in the age hardenable AlCuMg 2024 alloy, *J. Mater. Sci.* 35 (2000) 4667–4672, doi:10.1023/A:1004838619943.
- [33] J. Kansy, Microcomputer program for analysis of positron annihilation lifetime spectra, *Nucl. Instrum. Methods Phys. Res. A* 374 (1996) 235–244, doi:10.1016/0168-9002(96)00075-7.
- [34] M. Elsayed, R. Krause-Rehberg, O. Moutanabbir, W. Anwand, S. Richter, C. Hagedorn, Cu diffusion-induced vacancy-like defects in freestanding GaN, *N. J. Phys.* 13 (2011), doi:10.1088/1367-2630/13/1/013029.
- [35] J. Čížek, M. Vlček, I. Procházka, Digital spectrometer for coincidence measurement of Doppler broadening of positron annihilation radiation, *Nucl. Instrum. Methods Phys. Res. Sect. A Accel. Spectrom. Detect. Assoc. Equip.* 623 (2010) 982–994.
- [36] J. Čížek, M. Vlček, I. Procházka, Investigation of positron annihilation-in-flight using a digital coincidence Doppler broadening spectrometer, *N. J. Phys.* 14 (2012) 35005, doi:10.1088/1367-2630/14/3/035005.
- [37] G. Kresse, J. Hafner, *Ab-initio* molecular dynamics for liquid metals, *Phys. Rev. B* 47 (1993) 558–561, doi:10.1103/PhysRevB.47.558.
- [38] G. Kresse, J. Furthmüller, Efficient iterative schemes for *ab-initio* total-energy calculations using a plane-wave basis set, *Phys. Rev. B* 54 (1996) 11169–11186, doi:10.1103/PhysRevB.54.11169.
- [39] P.E. Blöchl, Projector augmented-wave method, *Phys. Rev. B* 50 (1994) 17953–17979, doi:10.1103/PhysRevB.50.17953.
- [40] G. Kresse, J. Hafner, Norm-conserving and ultrasoft pseudopotentials for first-row and transition elements, *J. Phys. Condens. Matter* 6 (1994) 8245–8257, doi:10.1088/0953-8984/6/40/015.
- [41] G. Kresse, D. Joubert, From ultrasoft pseudopotentials to the projector augmented-wave method, *Phys. Rev. B* 59 (1999) 1758–1775, doi:10.1103/PhysRevB.59.1758.
- [42] J.P. Perdew, K. Burke, M. Ernzerhof, Generalized gradient approximation made simple, *Phys. Rev. Lett.* 77 (1996) 3865–3868, doi:10.1103/PhysRevLett.77.3865.
- [43] M.J. Puska, R.M. Nieminen, Theory of positrons in solids and on solid surfaces, *Rev. Mod. Phys.* 66 (1994) 841–897, doi:10.1103/RevModPhys.66.841.
- [44] J.P. Desclaux, Hartree fock slater self consistent field calculations, *Comput. Phys. Commun.* 1 (1969) 216–222, doi:10.1016/0010-4655(70)90008-1.
- [45] J.P. Desclaux, A multiconfiguration relativistic DIRAC-FOCK program, *Comput. Phys. Commun.* 9 (1975) 31–45, doi:10.1016/0010-4655(75)90054-5.
- [46] A.P. Seitsonen, M.J. Puska, R.M. Nieminen, Real-space electronic-structure calculations: combination of the finite-difference and conjugate-gradient methods, *Phys. Rev. B* 51 (1995) 14057–14061, doi:10.1103/PhysRevB.51.14057.
- [47] E. Borowski, R.M. Nieminen, Electron-positron density-functional theory, *Phys. Rev. B* 34 (1986) 3820–3831, doi:10.1103/PhysRevB.34.3820.
- [48] W. Witt, Absolute Präzisionsbestimmung von gitterkonstanten an germanium- und aluminium-einkristallen mit elektroneninterferenzen, *Z. Naturforsch.* 22A (1967) 92–95.
- [49] J. Kuriplach, A.L. Morales, C. Dauwe, D. Segers, M. Šob, Vacancies and vacancy-oxygen complexes in silicon: positron annihilation with core electrons, *Phys. Rev. B* 58 (1998) 10475–10483, doi:10.1103/PhysRevB.58.10475.
- [50] S. Mantl, W. Triftshäuser, Defect annealing studies on metals by positron annihilation and electrical resistivity measurements, *Phys. Rev. B* 17 (1978) 1645–1652, doi:10.1103/PhysRevB.17.1645.
- [51] S. Linderth, H. Rajainmäki, R.M. Nieminen, Defect recovery in aluminum irradiated with positrons at 20 K, *Phys. Rev. B* 35 (1987) 5524–5528, doi:10.1103/PhysRevB.35.5524.
- [52] A.J. McAlister, D.J. Kahan, The Al-Sn (Aluminum-Tin) system, *Bull. Alloy Ph. Diagr.* 4 (1983) 410–414, doi:10.1007/BF02868095.
- [53] J.L. Murray, The Al-In (Aluminum-Indium) system, *Bull. Alloy Ph. Diagr.* 4 (1983) 271–278, doi:10.1007/BF02868666.
- [54] K. Carling, G. Wahnström, T.R. Mattsson, A.E. Mattsson, N. Sandberg, G. Grimvall, Vacancies in metals: from first-principles calculations to experimental data, *Phys. Rev. Lett.* 85 (2000) 3862–3865, doi:10.1103/PhysRevLett.85.3862.

- [55] J.A. Jackman, G.M. Hood, R.J. Schultz, Positron lifetime measurements of the vacancy properties of annealed and electron-irradiated aluminium, *J. Phys. F Met. Phys.* 17 (1987) 1817–1831, doi:[10.1088/0305-4608/17/9/009](https://doi.org/10.1088/0305-4608/17/9/009).
- [56] E. Gramsch, K.G. Lynn, Trapping model for thermal and nonthermal positrons in metals, *Phys. Rev. B* 40 (1989) 2537–2540, doi:[10.1103/PhysRevB.40.2537](https://doi.org/10.1103/PhysRevB.40.2537).
- [57] M. Elsayed, R. Krause-Rehberg, B. Korff, S. Richter, H.S. Leipner, Identification of As-vacancy complexes in Zn-diffused GaAs, *J. Appl. Phys.* 113 (2013), doi:[10.1063/1.4793791](https://doi.org/10.1063/1.4793791).
- [58] M.W. Thompson, *Defects and Radiation Damage in Metals*, Cambridge University Press, London, 1969.
- [59] D. Segers, F. Van Brabander, L. Dorikens-Vanpraet, M. Dorikens, Isothermal annealing of room temperature deformed iron studied with the positron annihilation technique, *Appl. Phys. A* 27 (1982) 129–132, doi:[10.1007/BF00616662](https://doi.org/10.1007/BF00616662).
- [60] A.N. Kolmogorov, On the statistical theory of the crystallization of metals, *Bull. Acad. Sci. USSR Math. Ser.* 1 (1937) 355–359.
- [61] W.A. Johnson, R.F. Mehl, Reaction kinetics in processes of nucleation and growth, *Am. Inst. Min. Metal. Petro. Eng.* 135 (1939) 416–458.
- [62] M. Avrami, Granulation, phase change, and microstructure kinetics of phase change. III, *J. Chem. Phys.* 9 (1941) 177–184, doi:[10.1063/1.1750872](https://doi.org/10.1063/1.1750872).
- [63] T. Angsten, T. Mayeshiba, H. Wu, D. Morgan, Elemental vacancy diffusion database from high-throughput first-principles calculations for FCC and HCP structures, *N. J. Phys.* 16 (2014) 15018, doi:[10.1088/1367-2630/16/1/015018](https://doi.org/10.1088/1367-2630/16/1/015018).
- [64] H. Ullmaier, Landolt-Börnstein, Numerical Data and Functional Relationships in Science and Technology, 25, Crystal and Solid State Physics, New Series, Group III, 1991 Atomic Defects in Metals, in: *Berichte Der Bunsengesellschaft Für Physikalische Chemie*, Springer-Verlag, Berlin, doi:[10.1002/bbpc.19930970923](https://doi.org/10.1002/bbpc.19930970923).